Nano Research 2017, 10(3): 1056–1063
DOI 10.1007/s12274-016-1366-5
Research Article

ISSN 1998-0124
CN 11-5974/O4

Nanosphere molecularly imprinted polymers doped with gold nanoparticles for high selectivity molecular sensors

Tehila Shahar, Tama Sicron, and Daniel Mandler (✉)

Institute of Chemistry, The Hebrew University of Jerusalem, Jerusalem 9190401, Israel

Received: 24 September 2016
Revised: 4 November 2016
Accepted: 9 November 2016

KEYWORDS
molecularly imprinted polymers,
surface enhanced Raman scattering (SERS),
gold nanoparticles,
Sudan IV,
doping

ABSTRACT

We report the first attempt of using molecularly imprinted polymers (MIPs) in the shape of nanoparticles that were doped with gold nanoparticles (AuNPs) for surface enhanced Raman scattering (SERS)-based sensing of molecular species. Specifically, AuNPs doped molecularly imprinted nano-spheres (AuNPs@nanoMIPs) were synthesized by one-pot precipitation polymerization using Sudan IV as the template for the SERS sensing. The AuNPs@nanoMIPs were characterized by various modes of scanning transmission electron microscopy (STEM) that showed the exact location of the AuNPs inside the MIP particles. The effects of Au concentration and solution stirring on the shape and the polydispersity of the particles were studied. Significant enhancement of the Raman signals was observed only when the MIP particles were doped with the AuNPs. The SERS signal improved significantly with increase in the Au concentration inside the AuNPs@nanoMIPs. Selectivity measurements of the Sudan IV imprinted AuNPs@nanoMIPs carried out with different Sudan derivatives showed high selectivity of the AuNPs-doped MIP particles.

1 Introduction

One of the most important tools studied and developed for high selectivity sensing is molecularly imprinted polymers (MIPs), since they are tailor-made synthetic receptors that mimic biological systems, such as enzymes or antigens. The MIP is a 3D polymeric network with specific binding sites obtained by copolymerizing functional monomers and a cross-linker in the presence of a template molecule [1–3]. The latter is removed to form cavities that exhibit high affinity towards the template.

The main advantages of MIPs as compared to the biological systems are their ease of formation, low-cost, high stability, and the large collection of available monomers. On the other hand, the predominant disadvantage of MIPs is the sluggish kinetics of binding, i.e., the ingress and the egress of the target into and out of the recognition sites. This is due to the rigid cross-linked MIP network that retards the diffusion through the MIP matrix. This limitation can be addressed by synthesizing MIPs as particles instead of continuous films, which increases their surface area significantly. Furthermore, the fabrication of

Address correspondence to daniel.mandler@mail.huji.ac.il

nanostructured MIPs (nanoMIPs) enables their easier dispersion and attachment to nanometric patterns in various devices (e.g., sensors) [4].

Owing to their special characteristics, nanoMIPs have been integrated as receptors in a variety of chemical sensors based on three types of transducers namely, electrochemical (e.g., potentiometry [5], impedance [6], and voltammetry [7]), mass-sensitive (e.g., quartz crystal microbalance (QCM) [8]), and optical (e.g., luminescence [9], surface plasmon resonance (SPR) [10], and surface enhanced Raman scattering (SERS) [11]), where detection limits as low as few fM were reported [12]. Gold nanoparticles (AuNPs) are among the nanomaterials which are ideal photothermal mediators for SPR excitations [13]. The local field that is created due to the AuNPs polarizes the molecules in the vicinity of the AuNPs, which enhances the Raman signals by several orders of magnitude [14].

Recently two approaches have been used to embed AuNPs in the MIPs. The most common method involves the incorporation of the AuNPs in continuous thin films, i.e., AuNPs@MIPs. The purpose of introducing the AuNPs into the MIPs is to increase their conductivity as the doping can facilitate electron transfer, increase the electrode specific area, and catalyze the electrochemical reactions [14]. Hence, most of the previously reported studies are based on electrochemical detection [15–18]. Electropolymerized AuNPs@MIP films have also been combined with QCM [19] and applied for volatile analytes in the gaseous phase [20]. Optical sensing by SERS and SPR using AuNPs@MIP films has also been reported [21, 22].

The second embedding method is based on doping of colloidal (mostly micron size) MIPs with the AuNPs. These particulate composites are usually in the form of microgels or core–shell structures [23–26] and are typically applied by attaching them onto thin films.

To the best of our knowledge, only two studies that utilize dispersed MIPs doped with AuNPs for optical sensing have been previously reported. Both studies use core–shell structure. Bompart et al. [27] prepared submicron core–shell MIP by coating the polymeric particles with the AuNPs, which were further covered by a thin MIP film. The Au clusters acted as antennae and facilitated the SERS measurement of the target molecule, (S)-propranolol, with three orders of magnitude higher sensitivity compared to the measurements using undoped MIPs. They were the first to apply SERS for target detection using a single MIP core–shell particle. Later, Xue et al. [28] fabricated surface-imprinted core–shell AuNPs for the determination of bisphenol A using a portable Raman spectrometer. The target was covalently attached to the silica monomer and was later thermally removed to obtain rapid and selective binding of bisphenol A with high intensity-concentration linearity.

Herein, we present the one-pot controlled synthesis of nanoMIPs doped with AuNPs (AuNPs@nanoMIPs) for improved SERS sensing (Scheme 1). The two significant advantages of this method are the control over the amount of the AuNPs, which significantly affects the sensitivity, and the utilization of the entire nanoMIP matrix, which increases the number of accessible recognition sites.

2 Experimental

The nanoMIPs were synthesized via radical precipitation polymerization using methacrylic acid (MAA), ethylene glycol dimethacrylate (EGDMA), and 1,1′-azobis(cyclohexanecarbonitrile) (ABCN) as the functional monomer, the cross linker, and the initiator, respectively. The AuNPs were stabilized with 8-mercaptooctanoic acid (MOA), to facilitate their integration during polymerization by the supramolecular interaction with the MAA monomers. The diameter of the AuNPs is 8.3 ± 1.4 nm. The transmission electron microscope (TEM) images of the AuNPs are presented in Fig. S1 in the Electronic Supplementary Material (ESM). The detailed syntheses are available in the methods section in the ESM.

3 Results and discussion

3.1 Effect of Au concentration

Figures 1(a)–1(d) show the extra high-resolution scanning electron microscope (XR-SEM) images of the non-imprinted polymers (NIPs) at different concentrations of the AuNPs. The effect of the concentration of the AuNPs on the diameter of the NIPs is shown in Fig. 1(e). Evidently, the diameter of the

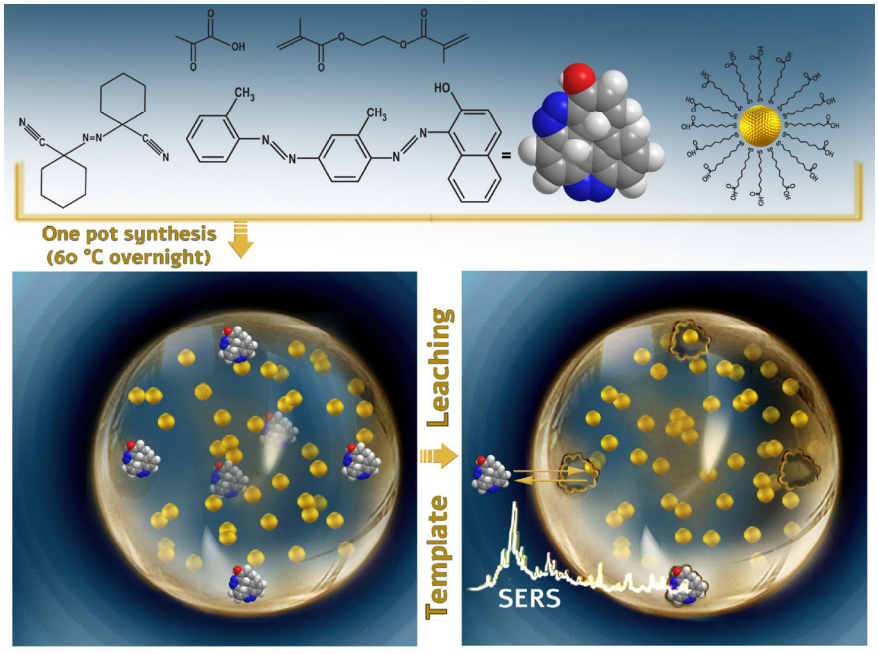

Scheme 1 Schematic of the one-pot controlled synthesis of AuNPs@nanoMIPs for improved SERS sensing.

particles decreases as the concentration of the AuNPs increases, which is in accordance with Ref. [29]. It is interesting to note that the AuNPs did not exist outside the NIP particles. This implies that the AuNPs functioned as seeds during the synthesis of the nanoMIPs. Thus, increasing the number of seeds raises the number of the MIP particles and consequently decreases their size. Furthermore, the NIPs obtained in the absence of the AuNPs are highly polydispersed with standard deviation (SD) of 75%, which decreases to approximately 9% in the presence of the AuNPs. The high SD is a result of two MIP populations (Fig. 1(a)). We have recently shown [30] that chloroform (a θ-solvent) yielded two populations of highly polydispersed MIP particles. We believe that the strong hydrogen bonding between the stabilization group of the AuNPs, MOA, and the functional monomer of the MIP, MAA, results in the growth of monodispersed AuNPs@nanoMIPs.

A clear evidence of the successful doping was obtained by the energy dispersive X-ray analyses (EDX) of the AuNPs@nanoNIPs and the undoped NIPs, and summarized in Table S1 in the ESM. The Fourier transform infrared (FTIR) spectra were recorded for the doped and the undoped MIPs and are presented in Fig. S4 in the ESM.

3.2 Effect of stirring

The various parameters affecting the shape, the diameter, and the polydispersity of the particles were examined. These include the nature of the solvent (acetonitrile and tetrahydrofuran in different ratios, which were not as good as chloroform) and the stirring of the solution during the polymerization. Figure 2 shows the XR-SEM images of the AuNPs@nanoNIPs prepared with and without stirring of the solution. The average diameters of the particles obtained from the stirred and the non-stirred solutions are 360 ± 46 (12.8% SD) and 2,134 ± 1,371 nm (64.2% SD), respectively, which indicates that the process of stirring significantly decreases the diameter and the polydispersity of the particles. This observation is in agreement with previous studies that show an exponential relationship between the weight-average diameter and the stirring rate [31].

3.3 STEM analyses

In order to obtain a better image of the AuNPs@nanoMIPs and to validate the presence of the AuNPs inside, we sliced the MIPs using a microtome (see the ESM). The thin slices were placed on a TEM grid and characterized using different modes of STEM, i.e., bright field (BF), dark field (DF), and high angle

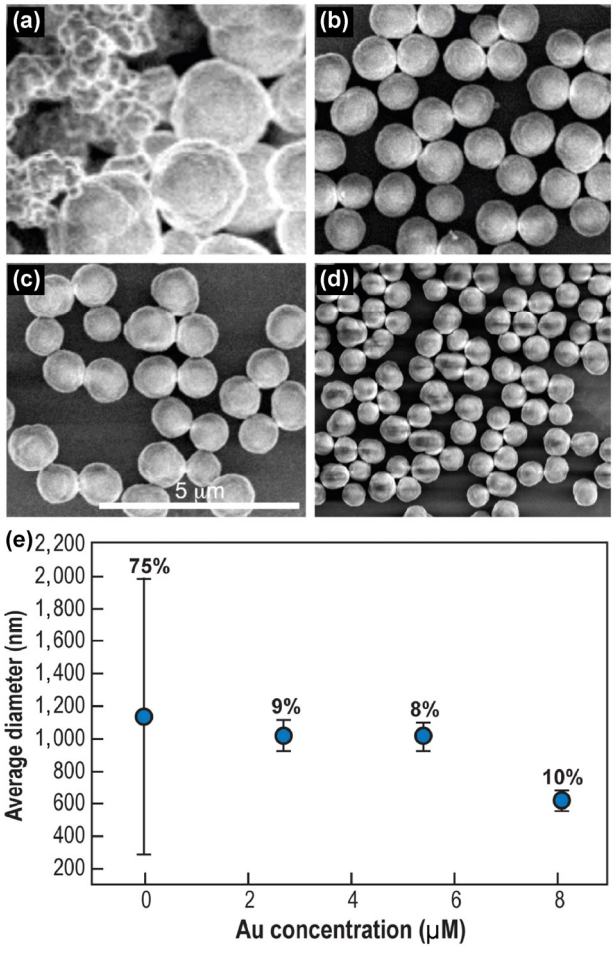

Figure 1 XR-SEM images of AuNPs@nanoNIPs at Au concentrations of (a) 0, (b) 2.7, (c) 5.4, and (d) 8.1 μM. (e) Average diameter of the AuNPs@nanoNIPs as a function of the Au concentration. The %SD is indicated next to each data point. The particles size distribution was analyzed as detailed in Fig. S2 in the ESM.

annular dark field (HAADF), as displayed in Fig. 3. Important information can be obtained by comparing the contrast of the three modes. Specifically, heavier atoms exhibit dark contrast in the BF image but bright contrast in the DF and the HAADF images. The latter is more sensitive to the atomic number "Z" since the HAADF detector collects the reflected beams from the widest angles. The DF detector collects the electrons scattered at narrower angles, and hence gives an image with better contrast. The various TEM images clearly show that the AuNPs are embedded in the MIPs. However, the distribution of the AuNPs inside the MIPs appears to be inhomogeneous (higher at the center). Therefore, a clear picture of the distribution is not obtained by TEM as it does not take into account

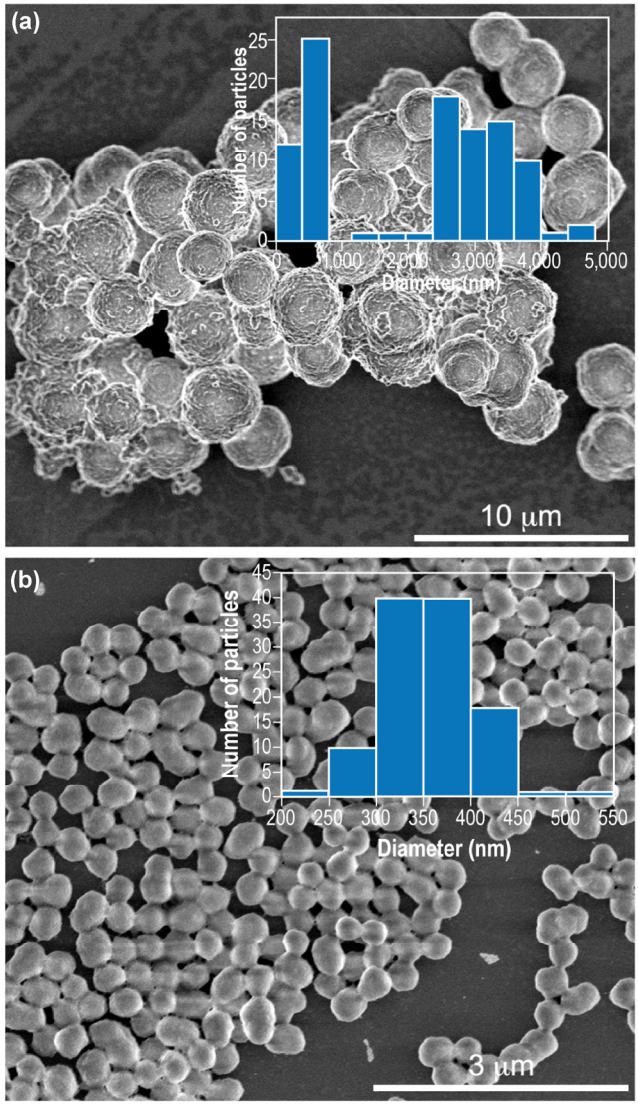

Figure 2 XR-SEM images of the AuNPs@nanoMIPs fabricated (a) without stirring and (b) with stirring. The inset shows the polydispersity of the particle diameter.

the spherical shape of the particles. In other words, the TEM image gives a 2D presentation of all the AuNPs in one MIP particle.

3.4 SERS measurements

SERS measurements were conducted using the sliced MIP particles placed on a gilded TEM grid (see Fig. S3 in the ESM for the typical optical microscopy image). As a model system, we selected Sudan dyes as target molecules. Lately, these dyes were banned by the European Union, as they were classified as carcinogens of the third degree by the International Agency for

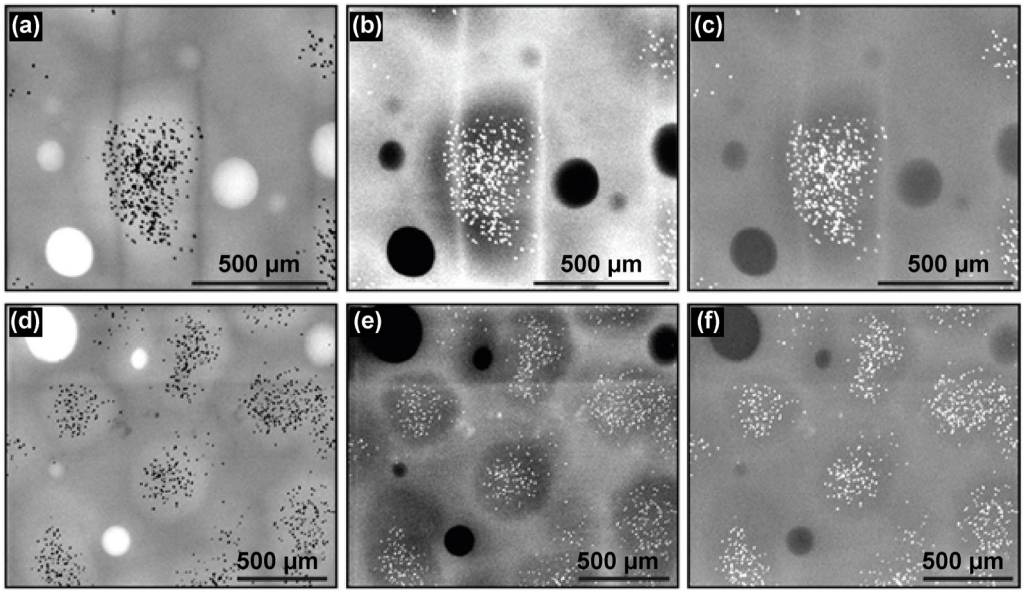

Figure 3 XR-STEM images of the AuNPs@nanoMIPs acquired using the three modes: BF ((a) and (d)), DF ((b) and (e)), and HAADF ((c) and (f)). The MIPs were sliced using a microtome and placed on a TEM grid. The concentrations of the AuNPs and Sudan IV, respectively are ((a)–(c)) 33 μM and 2.1 mM, and ((d)–(f)) 50 μM and 1.6 mM. The white ((a) and (d)) and black ((b), (c), (e), and (f)) disks are holes in the epoxy resin created by the bubbles trapped inside during solidification.

Research on Cancer. However, the food industry still uses them illegally for coloring chili and tomato sauces [32, 33]. Moreover, these dyes exhibit well-defined Raman spectra, without the effect of fluorescence. Figure 4(a) shows the Raman spectra of the undoped NIPs, the MIPs imprinted with Sudan IV (the molecular structure is shown in the inset of Fig. 4(a)), AuNPs@nanoNIPs and the AuNPs@nanoMIPs (at two different Au concentrations). The Raman spectra of all the samples were acquired before leaching the template. As can be seen, in the absence of the doped AuNPs there are no well-defined Raman shifts, even in the Sudan IV imprinted particles. Hence, it can be confirmed that the gilded substrate did not cause any surface enhancement. On the other hand, doping with the AuNPs resulted in Raman shifts, which are attributed to the molecules in proximity to the AuNPs, i.e., the MIP matrix and Sudan IV. Comparing Figs. 4(a1) and 4(a5), it is evident that doubling the concentration of the AuNPs significantly enhances the Raman signals and reveals additional spectroscopic features, as reported previously [27]. Figure 4(b) compares the spectra of the AuNPs@ nanoMIPs (imprinted with Sudan IV) and bulk Sudan IV (powder). It is evident that there are numerous Raman bands that appear in the spectra of both the imprinted and the Sudan IV samples, clearly indicating the presence of the dye in the imprinted particles (see the ESM).

3.5 Reuptake experiments

Reuptake experiments were carried out for the undoped and the AuNPs doped MIPs, i.e., leaching the template of the MIPs, and re-suspending them in the Sudan IV solution (as described in the Methods section in the ESM). The Raman spectra were acquired after slicing the particles and placing them on a gilded TEM grid. The Raman spectra of the AuNPs@nanoMIPs, the undoped MIPs and the epoxy background are presented in Fig. 4(c). The spectrum of the AuNPs@nanoMIPs is significantly more detailed and enhanced in comparison with the spectrum of the undoped MIPs. Most importantly, many bands that are associated with Sudan IV (see the ESM) were observed only in the spectrum of the AuNPs doped MIPs. The calculation of the enhancement factor per adsorbed molecule is difficult since it requires the determination of the quantity of Sudan IV absorbed on the gold surface (as also reported by Bompart et al. [27]).

The selectivity of the AuNPs@nanoMIPs imprinted with Sudan IV towards different Sudan derivatives,

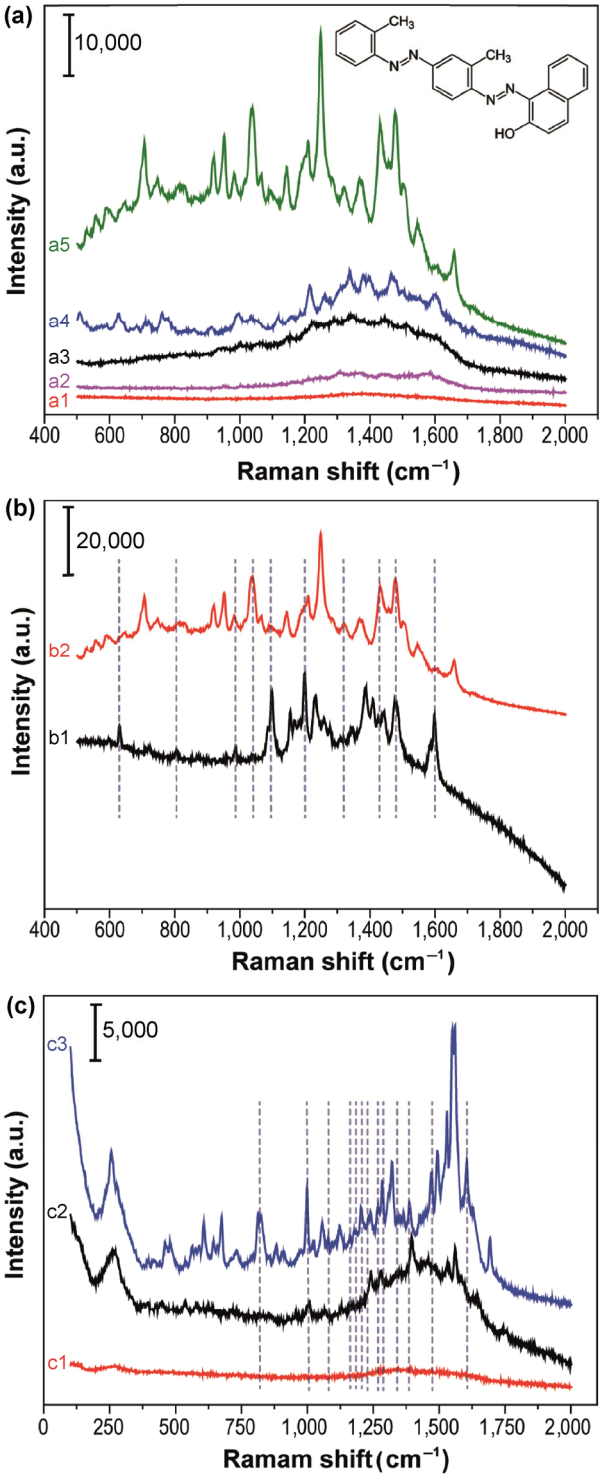

Figure 4 (a) SERS spectra of Sudan IV using (a1) nanoMIPs, (a2) AuNPs@nanoNIPs, (a3) nanoNIPs, (a4) AuNPs@nanoMIPs, and (a5) nanoMIPs doped with double the concentration of AuNPs. The inset shows the schematic of the molecular structure of Sudan IV. (b) SERS spectra of (b1) Sudan IV powder and (b2) AuNPs@nanoMIPs. (c) SERS spectra of (c1) epoxy, (c2) nano MIPs, and (c3) AuNPs@nanoMIPs after the reuptake experiments in Sudan IV solution.

i.e., Sudan II and Sudan III, was studied by applying the same reuptake procedure used for Sudan IV. Figure S5 in the ESM shows the Raman spectra acquired for the three samples. Sudan III, which has a very similar structure to Sudan IV, could not be detected and the spectrum obtained did not show any distinct Raman shifts. On the other hand, the spectrum of Sudan II showed Raman shifts of lower intensities and different frequencies as compared to the spectrum of Sudan IV. Some of the Raman features can be attributed to Sudan II, a smaller molecule that can enter the cavities in the MIP particles made by Sudan IV. Even though Sudan II can be detected, the dissimilarities in the Raman spectra can be used to differentiate between the different dyes.

4 Conclusions

In conclusion, AuNPs doped molecularly imprinted nano-spheres were fabricated by one-pot synthesis via precipitation polymerization for SERS sensing. The shape and the polydispersity of the particles were affected by the concentration of the AuNPs and the stirring of the solution. The sliced AuNPs@nanoMIPs were characterized using BF, DF, and HAADF modes of STEM, which showed the exact location of the AuNPs inside the MIP particles. Substantial enhancement of the Raman signals of the template, Sudan IV, was obtained only while using AuNPs doped MIP particles. In all the other samples (i.e., AuNPs@nanoNIPs and undoped NIPs and MIPs), Sudan IV could not be detected. Significant improvement in the SERS signal was observed with increase in the Au concentration. Furthermore, only the AuNPs@nanoMIPs showed Raman shifts assigned to Sudan IV in the reuptake experiments. The selectivity measurements of the Sudan IV imprinted AuNPs@nanoMIPs towards similar molecules, i.e., different Sudan derivatives, showed that the AuNPs@nanoMIPs were highly selective to Sudan IV than the other dyes (i.e., Sudan II and Sudan III). Sudan III could not be detected, while Sudan II showed weak Raman signals that were significantly different from those of Sudan IV. Thus, the AuNPs@nanoMIPs are easy to fabricate and exhibits SERS sensing with very high specificity and selectivity.

Acknowledgements

T. Shahar acknowledges the partial support by Teva Pharmaceutical Industries LTD. We are indebted to the Harvey M. Krueger Family Center for Nanoscience and Nanotechnology of the Hebrew University. Special thanks to Prof. Joel M. Harris from the University of Utah for his advice. This project is also partially supported by the Focal Technology Area through the Israel National Nanotechnology Initiative (INNI).

Electronic Supplementary Material: Supplementary material (AuNPs@nanoNIPs synthesis for the study of the effect of AuNPs concentration on AuNPs@nanoNIPs diameter and polydispersity, NIPs synthesis for the study of stirring effect on AuNPs@nanoNIPs diameter and polydispersity, TEM of AuNPs, MIPs size analysis, optical microscopy image of the sliced AuNPs@nanoMIPs, Raman of AuNPs@nanoMIPs after reuptaking different Sudan derivatives for selectivity measurement, and FTIR of doped and undoped MIPs) is available in the online version of this article at http://dx.doi.org/10.1007/s12274-016-1366-5.

References

[1] Cheong, W. J.; Yang, S. H.; Ali, F. Molecular imprinted polymers for separation science: A review of reviews. *J. Sep. Sci.* **2013**, *36*, 609–628.

[2] Taguchi, Y.; Takano, E.; Takeuchi, T. SPR sensing of bisphenol A using molecularly imprinted nanoparticles immobilized on slab optical waveguide with consecutive parallel Au and Ag deposition bands coexistent with bisphenol A-immobilized Au nanoparticles. *Langmuir* **2012**, *28*, 7083–7088.

[3] Yoshimatsu, K.; Reimhult, K.; Krozer, A.; Mosbach, K.; Sode, K.; Ye, L. Uniform molecularly imprinted microspheres and nanoparticles prepared by precipitation polymerization: The control of particle size suitable for different analytical applications. *Anal. Chim. Acta* **2007**, *584*, 112–121.

[4] Xie, C. G.; Zhang, Z. P.; Wang, D. P.; Guan, G. J.; Gao, D. M.; Liu, J. H. Surface molecular self-assembly strategy for TNT imprinting of polymer nanowire/nanotube arrays. *Anal. Chem.* **2006**, *78*, 8339–8346.

[5] Basozabal, I.; Guerreiro, A.; Gomez-Caballero, A.; Aranzazu Goicolea, M.; Barrio, R. J. Direct potentiometric quantification of histamine using solid-phase imprinted nanoparticles as recognition elements. *Biosens. Bioelectron.* **2014**, *58*, 138–144.

[6] Congur, G.; Senay, H.; Turkcan, C.; Canavar, E.; Erdem, A.; Akgol, S. Estrone specific molecularly imprinted polymeric nanospheres: Synthesis, characterization and applications for electrochemical sensor development. *Comb. Chem. High Throughput Screen.* **2013**, *16*, 503–510.

[7] Afkhami, A.; Ghaedi, H.; Madrakian, T.; Ahmadi, M.; Mahmood-Kashani, H. Fabrication of a new electrochemical sensor based on a new nano-molecularly imprinted polymer for highly selective and sensitive determination of tramadol in human urine samples. *Biosens. Bioelectron.* **2013**, *44*, 34–40.

[8] Sener, G.; Ozgur, E.; Yilmaz, E.; Uzun, L.; Say, R.; Denizli, A. Quartz crystal microbalance based nanosensor for lysozyme detection with lysozyme imprinted nanoparticles. *Biosens. Bioelectron.* **2010**, *26*, 815–821.

[9] Ivanova-Mitseva, P. K.; Guerreiro, A.; Piletska, E. V.; Whitcombe, M. J.; Zhou, Z. X.; Mitsev, P. A.; Davis, F.; Piletsky, S. A. Cubic molecularly imprinted polymer nanoparticles with a fluorescent core. *Angew. Chem., Int. Ed.* **2012**, *51*, 5196–5199.

[10] Sener, G.; Uzun, L.; Say, R.; Denizli, A. Use of molecular imprinted nanoparticles as biorecognition element on surface plasmon resonance sensor. *Sens. Actuators B Chem.* **2011**, *160*, 791–799.

[11] Chang, L. M.; Ding, Y.; Li, X. Surface molecular imprinting onto silver microspheres for surface enhanced Raman scattering applications. *Biosens. Bioelectron.* **2013**, *50*, 106–110.

[12] Wackerlig, J.; Lieberzeit, P. A. Molecularly imprinted polymer nanoparticles in chemical sensing-synthesis, characterisation and application. *Sens. Actuators B Chem.* **2015**, *207*, 144–157.

[13] Qiu, J. J.; Wei, W. D. Surface plasmon-mediated photothermal chemistry. *J. Phys. Chem. C* **2014**, *118*, 20735–20749.

[14] Ahmad, R.; Griffete, N.; Lamouri, A.; Felidj, N.; Chehimi, M. M.; Mangeney, C. Nanocomposites of gold nanoparticles@molecularly imprinted polymers: Chemistry, processing, and applications in sensors. *Chem. Mat.* **2015**, *27*, 5464–5478.

[15] Gholivand, M. B.; Torkashvand, M. The fabrication of a new electrochemical sensor based on electropolymerization of nanocomposite gold nanoparticle-molecularly imprinted polymer for determination of valganciclovir. *Mater. Sci. Eng. C* **2016**, *59*, 594–603.

[16] Wang, X. J.; Luo, C. N.; Li, L. L.; Duan, H. M. An ultrasensitive molecularly imprinted electrochemical sensor based on graphene oxide/carboxylated multiwalled carbon nanotube/ionic liquid/gold nanoparticle composites for vanillin analysis. *RSC Adv.* **2015**, *5*, 92932–92939.

[17] Peng, D. H.; Li, X.; Zhang, L. Z.; Gong, J. M. Novel visible-light-responsive photoelectrochemical sensor of 2,4-dichlorophenoxyacetic acid using molecularly imprinted

polymer/BiOI nanoflake arrays. *Electrochem. Commun.* **2014**, *47*, 9–12.

[18] Metzger, T. S.; Tel-Vered, R.; Willner, I. Controlled vectorial electron transfer and photoelectrochemical applications of layered relay/photosensitizer-imprinted Au nanoparticle architectures on electrodes. *Small* **2016**, *12*, 1605–1614.

[19] Kong, L. J.; Pan, M. F.; Fang, G. Z.; He, X. L.; Yang, Y. K.; Dai, J.; Wang, S. Molecularly imprinted quartz crystal microbalance sensor based on poly(*o*-aminothiophenol) membrane and Au nanoparticles for ractopamine determination. *Biosens. Bioelectron.* **2014**, *51*, 286–292.

[20] Iqbal, N.; Afzal, A.; Mujahid, A. Layer-by-layer assembly of low-temperature-imprinted poly(methacrylic acid)/gold nanoparticle hybrids for gaseous formaldehyde mass sensing. *RSC Adv.* **2014**, *4*, 43121–43130.

[21] Yao, T.; Gu, X.; Li, T. F.; Li, J. G.; Li, J.; Zhao, Z.; Wang, J.; Qin, Y. C.; She, Y. X. Enhancement of surface plasmon resonance signals using a MIP/GNPs/rGO nano-hybrid film for the rapid detection of ractopamine. *Biosens. Bioelectron.* **2016**, *75*, 96–100.

[22] Cennamo, N.; Donà, A.; Pallavicini, P.; D'Agostino, G.; Dacarro, G.; Zeni, L.; Pesavento, M. Sensitive detection of 2,4,6-trinitrotoluene by tridimensional monitoring of molecularly imprinted polymer with optical fiber and five-branched gold nanostars. *Sens. Actuators B Chem.* **2015**, *208*, 291–298.

[23] Ahmad, R.; Félidj, N.; Boubekeur-Lecaque, L.; Lau-Truong, S.; Gam-Derouich, S.; Decorse, P.; Lamouri, A.; Mangeney, C. Water-soluble plasmonic nanosensors with synthetic receptors for label-free detection of folic acid. *Chem. Commun.* **2015**, *51*, 9678–9681.

[24] Lv, Y. Q.; Qin, Y. T.; Svec, F.; Tan, T. W. Molecularly imprinted plasmonic nanosensor for selective SERS detection of protein biomarkers. *Biosens. Bioelectron.* **2016**, *80*, 433–441.

[25] Gültekin, A.; Ersöz, A.; Hür, D.; Sariözlü, N. Y.; Denizli, A.; Say, R. Gold nanoparticles having dipicolinic acid imprinted nanoshell for *Bacillus cereus* spores recognition. *Appl. Surf. Sci.* **2009**, *256*, 142–148.

[26] Gültekin, A.; Ersöz, A.; Denizli, A.; Say, R. Preparation of new molecularly imprinted nanosensor for cholic acid determination. *Sens. Actuators B Chem.* **2012**, *162*, 153–158.

[27] Bompart, M.; De Wilde, Y.; Haupt, K. Chemical nanosensors based on composite molecularly imprinted polymer particles and surface-enhanced Raman scattering. *Adv. Mater.* **2010**, *22*, 2343–2348.

[28] Xue, J. Q.; Li, D. W.; Qu, L. L.; Long, Y. T. Surface-imprinted core-shell Au nanoparticles for selective detection of bisphenol a based on surface-enhanced Raman scattering. *Anal. Chim. Acta* **2013**, *777*, 57–62.

[29] Rauh, A.; Honold, T.; Karg, M. Seeded precipitation polymerization for the synthesis of gold-hydrogel core-shell particles: The role of surface functionalization and seed concentration. *Colloid Polym. Sci.* **2016**, *294*, 37–47.

[30] Shahar, T.; Tal, N.; Mandler, D. Molecularly imprinted polymer particles: Formation, characterization and application. *Colloids Surf. A-Physicochem. Eng. Asp.* **2016**, *495*, 11–19.

[31] Zhang, X. X.; Fan, Y. F.; Tao, X. M.; Yick, K. L. Fabrication and properties of microcapsules and nanocapsules containing *n*-octadecane. *Mater. Chem. Phys.* **2004**, *88*, 300–307.

[32] Rezaei, B.; Boroujeni, M. K.; Ensafi, A. A. Development of sudan II sensor based on modified treated pencil graphite electrode with DNA, o-phenylenediamine, and gold nano-particle bioimprinted polymer. *Sens. Actuators B Chem.* **2016**, *222*, 849–856.

[33] Kou, X.; Lei, J. D.; Geng, L. Y.; Deng, H. Q.; Jiang, Q. Y.; Zhang, G. F.; Ma, G. H.; Su, Z. G. Synthesis, characterization and adsorption behavior of molecularly imprinted nanospheres for erythromycin using precipitation polymerization. *J. Nanosci. Nanotechnol.* **2012**, *12*, 7388–7394.